



**HAL**  
open science

## Quasi-ordered C<sub>60</sub> molecular films grown on the pseudo-ten-fold (100) surface of the Al<sub>13</sub>Co<sub>4</sub> quasicrystalline approximant

Vincent Fournée, Emilie Gaudry, Julian Ledieu, Marie-Cécile de Weerd, R D Diehl

► **To cite this version:**

Vincent Fournée, Emilie Gaudry, Julian Ledieu, Marie-Cécile de Weerd, R D Diehl. Quasi-ordered C<sub>60</sub> molecular films grown on the pseudo-ten-fold (100) surface of the Al<sub>13</sub>Co<sub>4</sub> quasicrystalline approximant. *Journal of Physics: Condensed Matter*, 2016, 28 (355001), 10.1088/0953-8984/28/35/355001. hal-01379677

**HAL Id: hal-01379677**

**<https://hal.science/hal-01379677v1>**

Submitted on 11 Oct 2016

**HAL** is a multi-disciplinary open access archive for the deposit and dissemination of scientific research documents, whether they are published or not. The documents may come from teaching and research institutions in France or abroad, or from public or private research centers.

L'archive ouverte pluridisciplinaire **HAL**, est destinée au dépôt et à la diffusion de documents scientifiques de niveau recherche, publiés ou non, émanant des établissements d'enseignement et de recherche français ou étrangers, des laboratoires publics ou privés.

# Quasi-ordered C<sub>60</sub> molecular films grown on the pseudo-ten-fold (100) surface of the Al<sub>13</sub>Co<sub>4</sub> quasicrystalline approximant

V. Fournée<sup>a,1</sup>, É. Gaudry,<sup>1</sup> J. Ledieu,<sup>1</sup> M.-C. de Weerd,<sup>1</sup> and R. D. Diehl<sup>2</sup>

<sup>1</sup>*Institut Jean Lamour (UMR7198 CNRS-Nancy-Université de Lorraine), Parc de Saurupt, 54011 Nancy Cedex, France*

<sup>2</sup>*Department of Physics, Penn State University, University Park, PA 16802, USA*

(Dated: June 20, 2016)

The growth of C<sub>60</sub> films on the pseudo-ten-fold (100) surface of the orthorhombic Al<sub>13</sub>Co<sub>4</sub> quasicrystalline approximant was studied experimentally by scanning tunneling microscopy, low-energy electron diffraction and photoemission spectroscopy. The (100) surface terminates at bulk-planes presenting local atomic configurations with five-fold symmetry - similar to quasicrystalline surfaces. While the films deposited at room temperature were found disordered, high-temperature growth (up to 693 K) led to quasi-ordered molecular films templated on the substrate rectangular unit mesh. The most probable adsorption sites and geometries were investigated by density functional theory (DFT) calculations. A large range of adsorption energies was determined, influenced by both symmetry and size matching at the molecule-substrate interface. The quasi-ordered structure of the film can be explained by C<sub>60</sub> adsorption at the strongest adsorption sites which are too far apart compared to the distance minimizing the intermolecular interactions, resulting in some disorder in the film structure at a local scale. Valence band photoemission indicates a broadening of the molecular orbitals resulting from hybridization between the substrate and overlayer electronic states. Dosing the film at temperature above 693 K led to molecular damage and formation of carbide thin films possessing no azimuthal order with respect to the substrate.

PACS numbers: 68.35.bd, 68.37.Ef, 71.15.Mb, 71.20.Be

---

<sup>a</sup> Corresponding author. e-mail: vincent.fournee@univ-lorraine.fr

## I. INTRODUCTION

The growth of  $C_{60}$  films on metal surfaces has attracted much interest since the mid-nineties, motivated by possible applications in molecular electronics [1]. One important aspect is to understand the substrate-induced modifications of the electronic and structural properties of the  $C_{60}$  films. It is known that  $C_{60}$  molecules interact quite strongly with metal and semiconductor surfaces through different bonding mechanisms, from predominantly ionic to predominantly covalent bonding, associated with different degrees of charge transfer between the substrate and the molecules [2, 3]. This leads to a wide range of bonding strengths, from freely diffusing and rotating molecules at room temperature on one end [4, 5] to strongly bounded and rotationally frozen molecules with well-defined orientation with respect to the surface on the other end [6, 7]. It is also important to study the interplay between intermolecular (lateral) interactions and molecule-substrate (vertical) interactions in determining the structure of the  $C_{60}$  monolayer and its properties [8]. The growth of  $C_{60}$  monolayers on low index surfaces is well documented for metals like Ag [9–11], Au [9, 12], Cu [13], Ni [14], Pt [15, 16] or Pd [17]. On the closed-packed substrates, the molecules generally tend to form hexagonal arrangements in order to optimize their lateral interactions with a nearest-neighbor distance close to 1 nm found in bulk  $C_{60}$ . Distortions from the perfect hexagonal closed-packed (hcp) arrangement are observed in systems where the molecule-substrate interactions are strong and where lattice mismatch exists. This can lead to highly strained  $C_{60}$  monolayers and anisotropic nearest-neighbor (NN) distances, which may increase along certain directions and decrease along others. However the contraction of the NN distance is limited due to the steepness of the repulsive part of the van der Waals interaction potential between the  $C_{60}$  molecules [11]. More complex structures are usually found on (100) and (110) surfaces, frequently associated with some restructuring of the substrate [16, 18].

In this paper we investigate the adsorption and growth of a  $C_{60}$  monolayer on the (100) surface of the  $Al_{13}Co_4$  quasicrystalline approximant. This compound is a complex metallic alloy with a large unit cell. It contains pentagonal bipyramid columnar clusters extending along the [100] direction [19]. Its (100) surface shows an almost pure Al plane but with a complex structure and local motifs presenting a five-fold symmetry [20–22]. Compared to simple metal surfaces, such types of surfaces exhibit a much more complex potential energy surface for any adsorbates landing on it. Therefore we expect that such a surface could serve as a template to grow molecular films with more complex structures than they usually do on simple metal surfaces. In the case of  $C_{60}$ , there is also the possibility that the five-fold symmetric motifs of the substrate could act as preferred adsorption sites through a symmetry matching with the pentagonal carbon faces of the molecule. Previous related studies dealt with the growth of  $C_{60}$  monolayers on the 5-fold surface of the Al-based icosahedral quasicrystals at room temperature. It was shown that in the low coverage regime, the  $C_{60}$  molecules tend to adsorb preferentially at specific quasilattice sites identified as dark stars in STM images [23]. At higher coverage however, the local order between the  $C_{60}$  molecules is quickly lost and the monolayer is disordered. A similar disordered phase has been observed on the 10-fold surface of the Al-Ni-Co decagonal phase [24]. Those results indicated a strong chemisorption of the molecules on these Al-based substrates. Other adsorption experiments were performed on either Pb or Bi pseudomorphic wetting layers deposited on the 10-fold surface of the Al-Ni-Co decagonal phase, with the idea to reduce the molecule-substrate interaction [25, 26]. In both cases, the mobility of adsorbed  $C_{60}$  molecules was much higher and resulted in the formation of *hcp* domains with no preferred orientation of the  $C_{60}$  lattice relative to the substrate lattice. More recently we have shown that molecular films with long-range quasiperiodic order can be grown by dosing the  $C_{60}$  molecules at elevated temperature [27]. This was demonstrated for different Al-based quasicrystalline substrates. The order is mediated by preferred adsorption of the  $C_{60}$  molecules with a pentagonal face on top of a local five-fold symmetric site [27, 28]. For similar growth conditions, a novel  $C_{60}$  superstructure has also been reported on the  $Al_9Co_2(001)$  surface, a related intermetallic [29]. The unit mesh contained six molecules and *ab initio* calculations showed that they adopt two main adsorption configurations on the intermetallic substrate. These first results demonstrate that complex metallic alloy surfaces can effectively act as a template to grow molecular films with novel structures. Here, we will show that a quasi-ordered molecular structure can be enforced in a  $C_{60}$  monolayer deposited on the  $Al_{13}Co_4(100)$  surface under appropriate growth conditions. The paper is organized as follows. A description of the methods is given in Sec. II. Then, we present the results in Sec. III, starting with a short description of the substrate structure, then a description of the nucleation and growth of the molecular film and ending with the report of carbide formation upon molecular decomposition at elevated temperature. The results are discussed in Sec. IV.

## II. METHODS

### A. Experimental details

The  $Al_{13}Co_4$  phase is an incongruently melting compound [30]. A single crystal of this phase was grown by the Czochralski method according to the previous work described by Gille *et. al* starting from an Al-rich solution [31].

First, an ingot with a composition of  $\text{Al}_{85}\text{Co}_{15}$  (in at.%) was prepared by induction melting under an inert Ar atmosphere. Then, the single crystal was pulled from the melted ingot with a constant rate of 0.5 mm/h. It had a diameter of up to 8 mm and was several centimeter in length. The Co content of the  $\text{Al}_{13}\text{Co}_4$  comprises between 23.9 and 24.4 at.% according to the phase diagram [30]. The single crystal was oriented by back-Laue scattering and cut perpendicular to its [100] pseudo-ten-fold axis. The surface of the oriented slice was then mechanically polished with diamond paste down to grain size  $0.25\ \mu\text{m}$  leading to a mirror-like appearance. A clean surface was prepared by repeated cycles of  $\text{Ar}^+$  sputtering (2 kV) and annealing (2 h at 1020 K) under ultra-high vacuum (UHV, base pressure  $1.10^{-10}$  mbar). The annealing temperature was measured using an optical pyrometer with the emissivity set to 0.35. The structural quality and the cleanliness of the surface was checked by low-energy electron diffraction (LEED), X-ray photoemission spectroscopy (XPS, Mg  $K\alpha$ ) and scanning tunneling microscopy (STM). STM images were recorded using a commercial Omicron VT-STM/AFM in constant current mode and processed using the WsXM software [32]. The 99.9+% pure  $\text{C}_{60}$  molecules from Alfa Aesar were sublimed from a Pyrex tube onto the surface by heating the tube to 513 K. Under these conditions, a complete  $\text{C}_{60}$  monolayer was deposited on the surface in 5 minutes. The coverages are given in terms of the saturated physical monolayer. Various deposition temperatures were tested; either room temperature or between 633 and 733 K. A second method was to dose the surface with a multilayer amount of  $\text{C}_{60}$  at room temperature and then anneal in the range of 633 to 733 K, which desorbed all  $\text{C}_{60}$  except for the first layer.

## B. Calculation details

We performed DFT calculations using the plane wave Vienna *ab initio* simulation package (VASP) [33–36]. The interaction between the valence electrons and the ionic core is described using the projector-augmented wave (PAW) method [37, 38] and the calculations are performed within the generalized gradient approximation (GGA-PBE) [39, 40]. To account for Van der Waals interactions, we used dispersion-corrected Kohn-Sham DFT energy functionals, where the conventional Kohn-Sham DFT energy functional is corrected by the DFT-D2 method [41]. Total energy calculations were realized using a cut of energy ( $E_{\text{cut}}$ ) equal to 450 eV and a  $k$ -points grid set to  $1 \times 3 \times 5$ . The surface was modeled with a 5-layer thick asymmetric slab built by bulk truncation. The slab is made of 3 fixed atomic layers at the bottom and 2 atomic layers allowed to relax. Two dense Al-rich surface models are considered in agreement with our previous study. The first one is a pure Al plane (labeled  $P_{\text{Al}}$ ) while in the second surface model Co atoms slightly below the mean position of the surface plane are present (labeled  $P_{\text{Al,Co}}$ ) [21]. A  $2 \times 1$  surface unit cell is required to ensure a sufficiently small coverage consistent with *a priori* weak interactions between adjacent molecules (the shortest distance between two molecules is around  $14.5\ \text{\AA}$ ). Such slabs already contain 308 atoms. The distance between two slab images is  $30 \simeq \text{\AA}$ . The adsorption energies are estimated from the evaluation of the total energy difference between the system  $\{\text{C}_{60}\text{ on Al}_{13}\text{Co}_4(001)\}$  and the sum of the systems  $\{\text{C}_{60}\}$  and  $\{\text{Al}_{13}\text{Co}_4(001)\}$ . These calculations are computationally demanding and therefore a limited number of adsorption sites have been tested, since our objective was not to get a precise picture of the surface properties towards  $\text{C}_{60}$  adsorption, but to draw a general picture and highlight some of the important parameters for  $\text{C}_{60}$  adsorption on complex surfaces.

## III. RESULTS

### A. The $\text{Al}_{13}\text{Co}_4(100)$ surface

The structure of the  $\text{Al}_{13}\text{Co}_4(100)$  surface has been investigated previously using a combination of experimental methods and *ab initio* calculations. The results have been reported in Ref. [20–22] and we summarize below the main conclusions pertaining to the present study. The orthorhombic  $\text{Al}_{13}\text{Co}_4$  compound crystallizes with space group  $Pmn2_1$  (oP102) and lattice parameters  $a = 0.8158\ \text{nm}$ ,  $b = 1.2342\ \text{nm}$  and  $c = 1.4452\ \text{nm}$ . [42] The unit cell contains 102 atoms. Similar to its parent decagonal quasicrystalline phase  $d\text{-AlNiCo}$  with  $8\ \text{\AA}$  periodicity, it has a four-layer periodicity along the pseudo-ten-fold [100] symmetry axis, with a stacking of flat ( $F$ ) and puckered ( $P$ ) planes. They appear in a sequence  $F_{0.0}P_{0.25}F_{0.5}P_{0.75}$  where  $P_{0.25}$  and  $P_{0.75}$  are mirrored against  $F_{0.5}$ . The bulk structure can be described by the packing of pentagonal bipyramid (PB) clusters extending along [100] and connected by glue atoms (see Fig. 1a) [19]. The equatorial planes of the PB clusters lie in the  $F$  planes while the top and bottom caps of the PB clusters lie in the  $P$  layers. Within each  $P$  layer, one find two sets of bipentagonal motifs corresponding to adjacent like caps of PB clusters (Fig. 1b). Caps consist of Al pentagonal rings centered by a Co atom. The Co atoms are slightly displaced above (top cap) or below (bottom cap) the Al pentagonal ring.

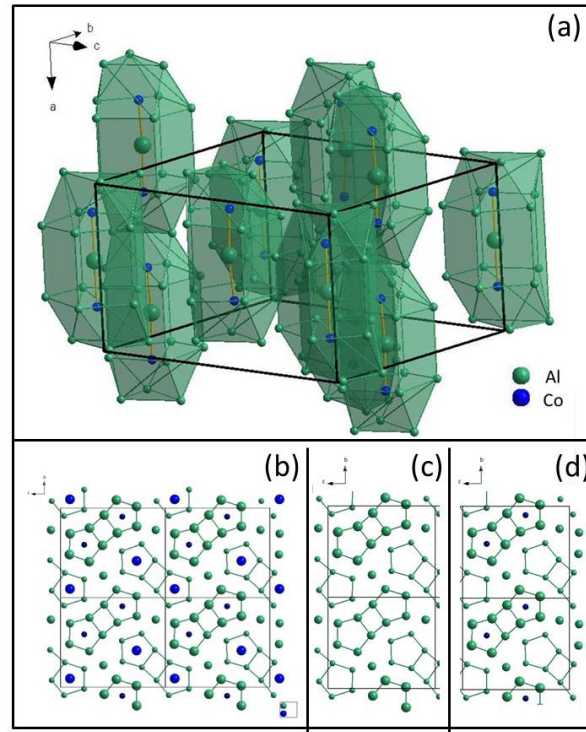


FIG. 1. (a) 3D view of the  $\text{Al}_{13}\text{Co}_4$  crystal structure where both the Co-Al-Co groups and the cages are displayed. (b) Model of the complete puckered layer perpendicular to the [100] axis. The green spheres represent Al atoms and the blue spheres Co atoms. Larger spheres stand for atoms protruding above the mean plane position and smaller spheres for atoms that are slightly below the mean plane position. The bipentagonal motifs are displayed. (c) Best-fit model according to Ref. [21] of the surface termination where all Co atoms of the puckered layer are missing. The model is referred to  $P_{\text{Al}}$ . (d) Model  $P_{\text{Al,Co}}$  containing all Al atoms as well as the Co atoms slightly below the mean position of the surface plane. The protruding Al bipentagonal are the main features imaged by STM as illustrated in Fig. 2(a) although all Al atoms are present.

Experimentally, it is found that the surface terminates at incomplete  $P$  layers [20–22]. Two sets of experiments performed on two different samples led to the conclusion that the exact structure of the terminating planes is sample dependent. A first report by Addou *et al.* indicated a surface consisting of  $P$  layers where only one set of bipentagonal motifs remain corresponding to the bottom caps of the PB clusters [20]. A second report by Shin *et al.* found that the surface consisted of  $P$  layers where the two sets of bipentagonal motifs remained but without (most of) the Co atoms, especially the protruding Co atoms of the top caps (Fig. 1c) [21]. Although both sets of bipentagonal motifs are present as evidenced by dynamical LEED and density functional theory (DFT) calculations, only one set of bipentagonal motifs is visible in STM images of this surface. This is shown in Fig. 2a. The bipentagonal motifs correspond to bottom caps of PB clusters having the Al pentagonal rings lying slightly above the mean position of the plane, while those of top caps lie slightly below and are not properly imaged by STM. Density functional theory calculations of relative surface energies of asymmetric slabs corresponding to different surface models have been calculated as a function of the chemical potential  $\mu_{\text{Al}}$  of Al in the alloy.[21] The allowable range of  $\mu_{\text{Al}}$  is determined by the condition of thermal equilibrium between surface and bulk ( $\mu_{\text{Al}_{13}\text{Co}_4} = 13\mu_{\text{Al}} + 4\mu_{\text{Co}}$ ) and the alloy stability ( $\Delta H_f \leq 0$ ) which results in  $\Delta H_f / 13 \leq \mu_{\text{Al}} - \mu_{\text{Al}}^{\text{bulk}} \leq 0$ . It is found that the two observed surface structures for the two different crystals correspond to two models having the lowest surface energies but for different range of  $\mu_{\text{Al}}$ . The different surface structures reported in Addou *et al.* and in Shin *et al.* might thus be explained by small differences in bulk chemical composition around stoichiometry that leads to a discontinuity in  $\mu_{\text{Al}}$  and thus to one surface termination or the other. In the following, we use the same single crystal as in Shin *et al.*[21], *i.e.* a surface terminating at  $P$  layers where (most) of the Co atoms have desorbed but (almost) all Al atoms remain. The structure model of this surface is shown in Fig. 1c. High-resolution STM images and corresponding fast-Fourier transform (FFT) of the substrate before  $\text{C}_{60}$  deposition are shown in Fig. 2(a,d). The protruding Al bipentagonal are the main features imaged by STM as can be seen in Fig. 2a

## B. Structure of $C_{60}$ monolayer upon room temperature deposition

A  $C_{60}$  monolayer was first deposited on the substrate held at room temperature. An STM image of the film is shown (Fig. 2b) together with the corresponding FFT (Fig. 2e). The film is found to be disordered as confirmed by the absence of diffraction spots in the LEED patterns after completion of the monolayer. Figure 2c shows an STM image of the same film after annealing at 633 K for 1 min. At this stage, a faint diffuse ring is observed in the FFT. The radius of this ring corresponds to a real space distance of about 1 nm which is consistent with the typical intermolecular distance measured in  $C_{60}$  films (Fig. 2f). Intermolecular distances can also be extracted directly from STM images. It indicates a tendency to form a closed packed hexagonal structure on a local scale (see inset of Fig. 2c). This is similar to what has already been reported for  $C_{60}$  film grown at room temperature on related Al-based quasicrystalline surface and was attributed to strong molecule-substrate interaction limiting surface diffusion leading to the lack of long-range order [23, 25, 43].

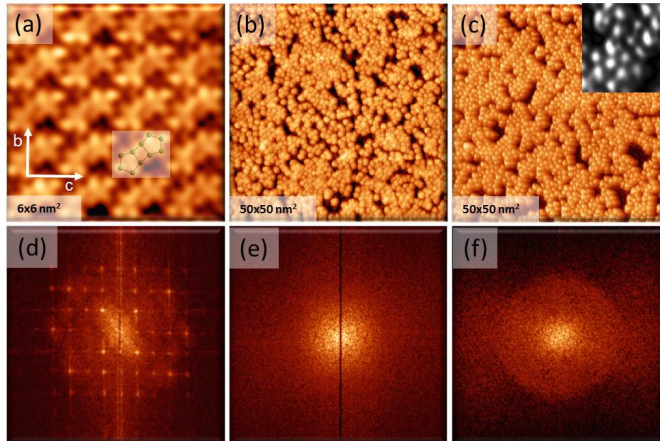


FIG. 2. (a) STM images ( $I_t=0.1$  nA,  $V_b=-0.6$  V) of the clean  $Al_{13}Co_4(100)$  surface. A schematic of the protruding bipentagonal motif is represented as well as the surface unit cell. (b) STM images ( $I_t=0.1$  nA,  $V_b=+2$  V) of the surface dosed with 0.95 ML of  $C_{60}$  at room temperature and (c) after annealing the later to 633 K. The inset in (c) shows local *hcp* packing (image size is  $5.7 \times 5.7$  nm<sup>2</sup>). (d-f) shows the FFT of STM images (a-c). The orthorhombic pattern (d) disappears completely after room temperature deposition of a complete ML (e) and a faint diffuse ring reappears after annealing at 633 K (f).

## C. Low coverage structure of $C_{60}$ monolayer upon high temperature deposition

In this section, we present results for films deposited on substrate held at elevated temperature with the aim to increase surface diffusion and improve structural order. To optimize the deposition temperature, a monolayer was first deposited at room temperature and then annealed sequentially. The annealing time was 5 min for each step and the C *1s* and Al *2p* XPS core-level spectra were recorded after each step. An additional component in the C *1s* peak was found to appear at 282 eV binding energy for annealing temperatures above 693 K as will be shown later, indicating molecular damage. This temperature was thus determined as the highest possible deposition temperature for thin film growth.

Figure 3 shows an STM image of the surface partially covered by  $C_{60}$  islands formed at a substrate temperature of 693 K. Molecular islands grow either from step edges or on terraces. Individual molecules are also observed. They might be molecules trapped at some specific adsorption sites or at some surface defect sites. Height histograms of STM images indicate an average height of the molecules of  $0.5 \pm 0.05$  nm measured with respect to the average substrate height, in the lower range of typical values reported for  $C_{60}$  on metal surfaces. This value does not change with the bias. On large scale images like in Fig. 3b, islands appear elongated according to specific directions, alternating on adjacent terraces from approximately  $[011]$  to  $[0\bar{1}\bar{1}]$  directions. This is reminiscent of the fact that two consecutive P layers along the  $[100]$  direction are mirrored from each other against the intermediate F layer. As a result, the protruding bipentagonal motifs observed on one terrace (see Fig. 2a) will appear rotated on the adjacent terrace. The fact that the elongation of the  $C_{60}$  islands follows the same orientation as that of protruding bipentagonal motifs demonstrates the influence of the atomic scale structure of the substrate on the film at this deposition temperature.



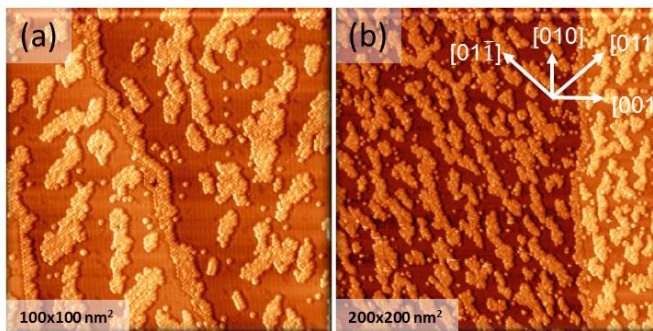


FIG. 3. (a, b) STM images of the  $C_{60}$  film dosed at 693 K showing submonolayer coverage on the  $Al_{13}Co_4(100)$  surface ( $I_t=0.1$  nA,  $V_b=+2$  V). The molecular islands appear elongated either along the  $[011]$  or  $[01\bar{1}]$  directions on adjacent terraces.

Low coverage experiments (a few percent of a monolayer) were performed in an attempt to determine preferred adsorption sites. High-resolution STM images allow to resolve both the substrate structure and the position of individual molecules as shown in Fig.4. The surface structure model can then be superimposed on the image with proper scaling. Each bright protrusion corresponds to an individual  $C_{60}$  having an apparent diameter of about 1.3 nm due to the tip convolution effect. Because of this large size, comparable to the substrate unit cell dimensions, it is actually impossible to precisely ascribe the position of the center of a molecule on a specific adsorption site simply from the experimental images. Examination of a number of STM images seems to indicate that there maybe not a single preferred adsorption sites but several. In case two molecules are found adjacent to each other, an intermolecular distance of  $\sim 1$  nm is measured, typical for  $C_{60}$  films on metal surfaces.

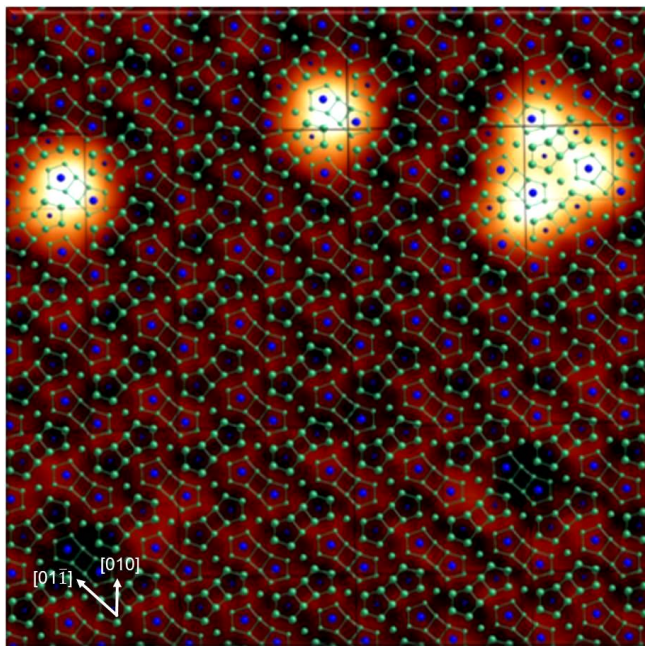


FIG. 4. STM image ( $10.5 \times 10.5$  nm<sup>2</sup>) showing individual  $C_{60}$  appearing as bright dots on the  $Al_{13}Co_4(100)$  surface at 693 K ( $I_t=0.1$  nA,  $V_b=+2$  V). The substrate structure with protruding BP motifs can still be observed and the model with BP motifs has been superimposed on the image.

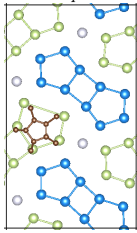
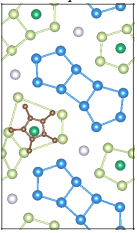
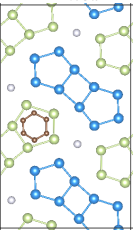
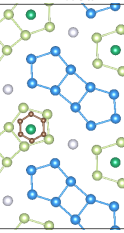
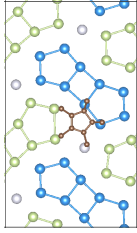
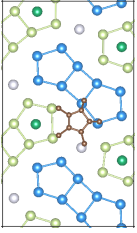
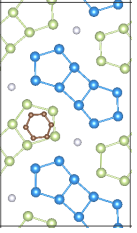
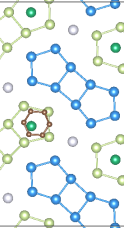
$P_{Al}$	$P_{Al,Co}$	$P_{Al}$	$P_{Al,Co}$
$5f A_{pent}^1$	$5f B_{pent}^1$	$5f A_{hex}^1$	$5f B_{hex}^1$
			
-1.93 eV	-1.70 eV	-1.50 eV	-1.53 eV
$5f A_{pent}^2$	$5f B_{pent}^2$	$5f A_{hex}^2$	$5f B_{hex}^2$
			
-2.86 eV	-3.02 eV	-1.73 eV	-1.89 eV

TABLE I. Adsorption geometries (top views) for a  $C_{60}$  molecule adsorbed in 5-fold adsorption sites. The topmost layer of the surface, represented in the figure, consists of two sets of bipentagonal motifs, slightly below (in light blue) or above (in light green) the mean position of the plane. The  $P_{Al,Co}$  surface model contains additional surface Co atoms (in dark green) located in the center of bipentagonal motifs. The  $C_{60}$  molecule is positioned with either one hexagonal or pentagonal ring facing the surface. Only the carbon atoms located close to the surface are represented (in brown). The black surface cell is  $14.4 \times 24.8 \text{ \AA}^2$ .

#### D. Adsorption energies and geometries

To get some insight into the possible adsorption geometries of  $C_{60}$  on this surface, adsorption energies have been calculated by DFT for different orientations of the molecules at several possible adsorption sites. We did not perform a systematic study because of the too large number of adsorption sites and geometries in this system. We have not considered neither possible surface reconstruction effects which could be induced by annealing the  $C_{60}$  film. Instead we have considered the most likely geometries based on symmetry matching. We call BP1 the bipentagonal motif lying slightly below the mean position of the plane and BP2 the bipentagonal motif lying slightly above. The BP2 motifs are the ones visible in STM images. For each adsorption configuration, two surface models are considered, differing only by the presence or absence of Co atoms slightly below the center of Al pentagonal rings forming the BP2 motifs. The two surface models present a similar surface structure with possible nearly 5-fold and 4-fold symmetric adsorption sites, located inside or in-between the bipentagonal motifs BP1 and BP2. The  $C_{60}$  molecule is positioned with either one hexagonal or pentagonal ring facing the surface. We have also considered the  $C_{60}$  molecule positioned with one C-C bonding [(5,6) or (6,6) bonds] facing the surface. However, the relaxations generally lead to a rotation of the  $C_{60}$  molecule which in the end will present an hexagonal ring facing the  $Al_{13}Co_4(100)$  surface. In one case, the molecule stayed with the (6,6) bond against the surface. However, the corresponding adsorption energy is quite high in this case (-1.55 eV).

##### *Adsorption in 5-fold sites*

The different adsorption geometries considered at 5-fold sites and the corresponding adsorption energies are gathered in table I. They range from -1.50 eV ( $5f A_{pent}^1$  site) to -3.02 eV ( $5f B_{pent}^2$  site). These two limiting values are obtained with the pentagonal face of the  $C_{60}$  molecule facing the  $Al_{13}Co_4(100)$  surface. A symmetry mismatch between the adsorption site and the molecular face against the surface leads to non favorable adsorption sites (energies in the range [-1.93 eV; -1.70 eV]). But symmetry matching alone is insufficient to ensure a favorable adsorption. The relative size between the pentagonal motifs of the site and of the molecule should be consistent. Indeed, a strong distortion of the bipentagonal motif is noticed when the  $C_{60}$  molecule is adsorbed in sites  $5f A_{pent}^1$  and  $5f B_{pent}^1$ , leading then to an unfavorable adsorption energy.



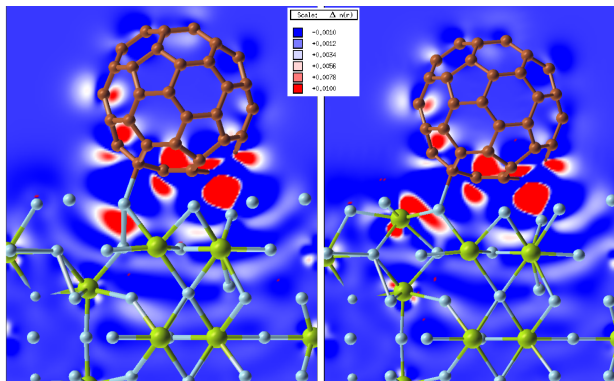


FIG. 5. Comparison of charge density differences for a  $C_{60}$  molecule adsorbed in  ${}^{5f}A_2$  (right) and  ${}^{5f}B_2$  (left). The scale is given in  $e/\text{\AA}^3$

The most favorable 5-fold adsorption site ( ${}^{5f}B_{pent}^2$ ) is located in between two bipentagonal motifs, roughly on top of an aluminum atom located in the subsurface (S-1 atomic plane). The shortest Al-C distances are between 2.00  $\text{\AA}$  and 2.20  $\text{\AA}$ . The surface Co atoms, located nearby, show a slight stabilizing effect: the energy difference between the two adsorption sites (with and without a Co atom nearby) is calculated to be 0.16 eV. They present a electronic donor character, highlighted by charge density deformation maps as shown in Fig.5.

#### Adsorption in 4-fold sites

The different adsorption geometries considered at 4-fold sites and the corresponding adsorption energies are gathered in table II. The 4-fold sites are more stable on average than the previous 5-fold sites: the adsorption energies are found in the range between -2.25 eV ( ${}^{4f}A_{hex}^1$  site) and -3.25 eV ( ${}^{4f}A_{hex}^{2'}$  site). Here again, both symmetry and size matching influence the adsorption energies: the unfavorable adsorption sites  ${}^{4f}A_{hex}^3$  and  ${}^{4f}A_{hex}^{3'}$  are ascribed to the distortion of the bipentagonal motif slightly above the mean position of the plane (BP2).

The two sets of bipentagonal motifs BP1 and BP2 are not equivalent regarding adsorption, even for the  $P_{Al}$  model which does not contain any surface Co atoms. It is more favorable to adsorb at BP1 motifs, *i.e.* in the depletion between protruding BP2 motifs. The adsorption energy differences can reach 1 eV ( ${}^{4f}A_{hex}^{1'}$  and  ${}^{4f}A_{hex}^{2'}$ ). The azimuthal orientation of the  $C_{60}$  molecule with respect to the surface normal is also crucial: energy differences calculated with the  $C_{60}$  molecule rotated by 90 degrees can reach 0.5 eV. This is linked to the number of Al-C bondings created at the surface (Fig. 6): only three charge accumulation lobes of charge density deformation are calculated for  ${}^{4f}B_{hex}^{1'}$  (resp.  ${}^{4f}B_{hex}^2$ ) while it is four for the rotated molecule ( ${}^{4f}B_{hex}^1$ , resp.  ${}^{4f}B_{hex}^{2'}$ ). However, the number of high charge accumulation areas for calculated charge deformation is not the unique key parameter to predict adsorption properties:  ${}^{4f}B_{hex}^1$  and  ${}^{4f}B_{hex}^{2'}$  present four such characteristics but corresponding adsorption energies differ by more than 0.8 eV.

The surface Co atoms have a weak influence on the calculated adsorption energies, with no clear trends in the adsorption energy differences calculated with either  $P_{Al,Co}$  or  $P_{Al}$  models in this case (absolute differences smaller than 0.3 eV).

The most stable sites are located in the center of the BP1 motif slightly below the mean plane position (type 2 adsorption sites, see Tab. II), with energy ranging from -3.14 eV ( ${}^{4f}A_{hex}^2$ ) to -3.31 eV ( ${}^{4f}B_{hex}^{2'}$ ), according to the molecular orientation and the surface model. In the case of the most favorable configuration ( ${}^{4f}B_{hex}^{2'}$ ), the Al-C distances are quite small ( $\simeq 2.10$   $\text{\AA}$ ), and the surface Co atoms have a slight stabilizing effect ( $\simeq 0.1$  eV).

In conclusion, the most favorable calculated adsorption site is  ${}^{4f}B_{hex}^{2'}$ , located at the center of a bipentagonal motif. The corresponding adsorption energy is -3.31 eV, which is similar to the value calculated for  $C_{60}$  on 5-fold Al-Pd-Mn quasicrystalline surface (-3.20 eV) [27] and on  $Al_9Co_2$  compound (-3.18 eV) [29]. In the latter case, the most favorable adsorption site is also a 4-fold site, located just above a subsurface Co atom. The next most stable adsorption site is a 5-fold site located in-between two bipentagonal motifs (-3.02 eV). Here again, the number of high charge accumulation areas for calculated charge deformation is not the unique key parameter to predict adsorption properties (Fig. 6). Note that these calculated adsorption energies on Al-based complex metallic surfaces are rather large compared to typical adsorption energies on noble metal surfaces (similar methods give -1.4 to -1.7 eV on Ag(111) or Au(111) [44],

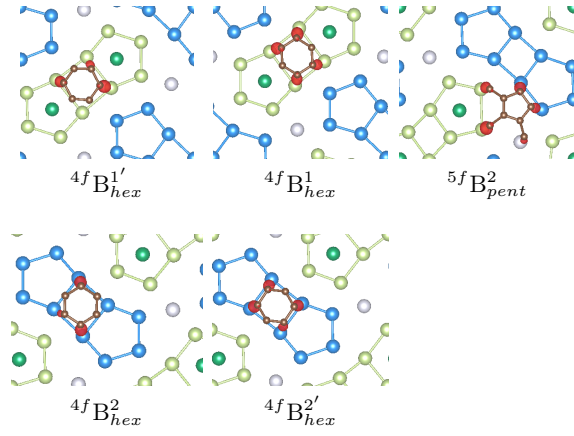


FIG. 6. Charge density deformation (isosurfaces  $0.1 e/\text{\AA}^3$ ).

-2.2 eV on Cu(111) [45]), for which the bonding type is predominantly ionic and of intermediate strength [46]. On Al(110) and (111) surfaces, the bonding type is predominantly covalent and characterized also as of intermediate strength, similar to noble metal surfaces [46]. The calculated bond strength for  $C_{60}$  on Al-based complex metallic surfaces is closer to those calculated for semiconductor surfaces (for example, -2.6 eV on Si(1x1)-(7x7) [47]). The shortest distances between C and substrate atoms are also smaller for Al-based CMA surfaces compared to other noble surfaces.

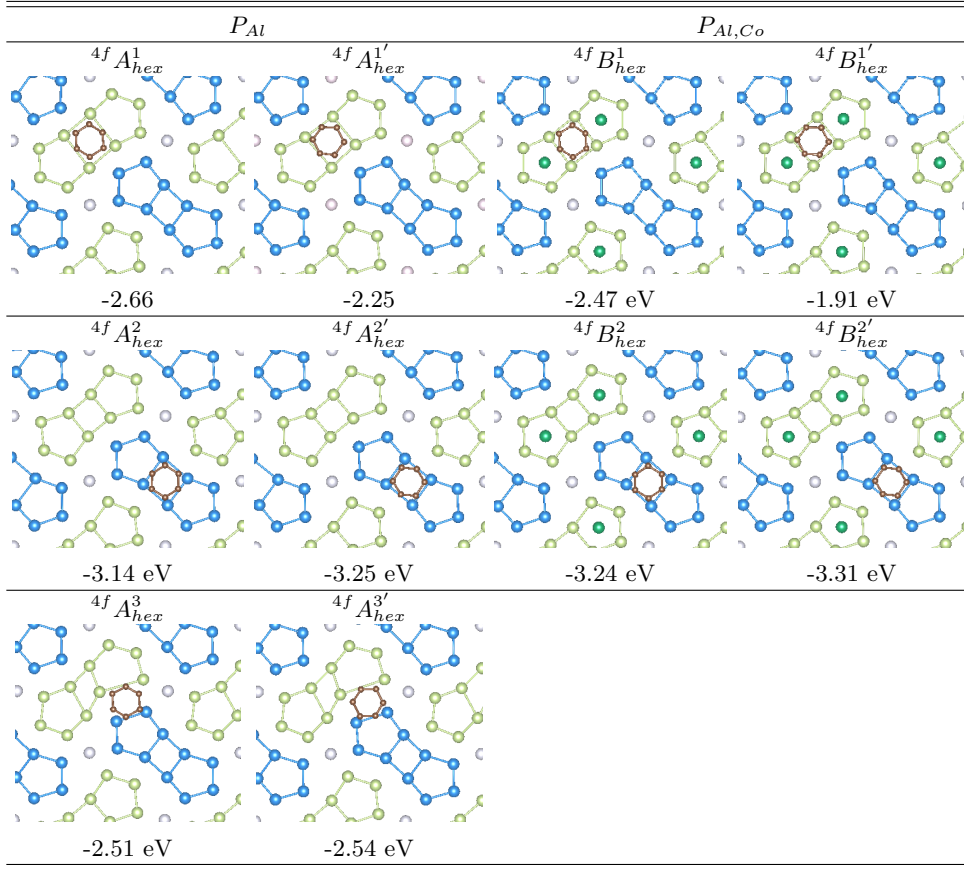


TABLE II. Adsorption geometries (top views  $21.6 \times 18.5 \text{ \AA}^2$ ) for a  $C_{60}$  molecule adsorbed in 4-fold adsorption sites. The topmost layer of the surface, represented in the figure, consists of two sets of bipentagonal motifs, slightly below (in light blue) or above (in light green) the mean position of the plane. The  $P_{Al,Co}$  surface model contains additional surface Co atoms (in dark green) located in the center of bipentagonal motifs. The  $C_{60}$  molecule is positioned with one hexagonal ring facing the surface, with two different orientations. Only the carbon atoms located close to the surface are represented (in brown).

### E. Structure of the monolayer upon high temperature deposition

The LEED pattern obtained after saturation of the monolayer deposited at 693 K shows an orthorhombic pattern similar to that of the substrate but with a higher background intensity (Fig. 7(a)). STM images of the corresponding film are shown in Fig. 7(a,b) at different length scales. It is obvious from these images that the molecular film is not perfectly ordered, but only quasi-ordered. The molecules tend to align preferentially along certain crystallographic directions of the substrate. On the particular terrace shown in Fig. 7(a,b), the molecular rows tend to align along the  $[01\bar{1}]$  direction, which is rotated anti-clockwise by  $49.5^\circ$  from the  $[010]$  direction. The shortest distances between two adjacent molecules along the  $[01\bar{1}]$  direction estimated from line profiles on STM images spread generally within  $1.0 \pm 0.1 \text{ nm}$ . The film also has significant rumpling, with a peak-to-peak roughness of 0.2 to 0.3 nm. More information on the film structure is obtained from the fast-Fourier transform (FFT) and the autocorrelation of STM images as shown in Fig. 7(c,d). The FFT has sharp spots located on a rectangular lattice having the same parameters as the substrate, consistent with the LEED pattern. It also contains some diffuse intensity located on both sides of each  $(1,1)$  spot and their equivalents, as well as inside the primary unit cell. This diffuse intensity could not be detected in the LEED pattern.

The STM autocorrelation shows intensity lines oriented along  $[01\bar{1}]$  and spaced by  $0.95 \pm 0.01 \text{ nm}$ , a distance equal to half the diagonal of the substrate unit cell (0.946nm). Clear maxima along these lines form a rectangular unit mesh having the same dimensions as that of the substrate (see inset of Fig. 7(d)). Additional diffuse intensity along the  $[01\bar{1}]$  diagonal indicates some occupation probability for an additional molecules along this diagonal, but its position is not well defined. The fact that the  $C_{60}$  molecules are preferentially aligned along the  $[01\bar{1}]$  direction on this particular terrace is reflected in spot intensities which are not equivalent in the FFT shown in Fig. 7(c) ( $(1,\bar{1})$  and  $(\bar{1},1)$  spots are more intense than  $(1,1)$  and  $(\bar{1},\bar{1})$  spots for example). In addition, some broad diffuse spots are

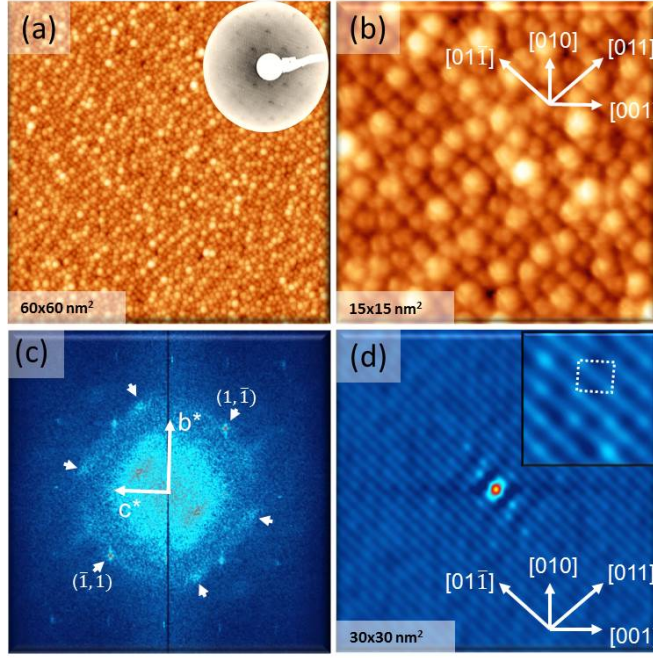


FIG. 7. (a, b) STM images of the complete  $C_{60}$  film deposited on the  $Al_{13}Co_4(100)$  surface at 693-713 K ( $I_t=0.1$  nA,  $V_b=+2$  V). The inset in (a) is LEED pattern of the film recorded at a beam energy of 23 eV. (c) FFT and (d) autocorrelation image of the film topographic image. The inset in (d) is  $6 \times 6$  nm<sup>2</sup>. The orthorhombic unit cell is shown as dotted lines.

distributed close to a circle intercepting the (1,1) and related spots and having a diameter 0.95 nm. These diffuse intensity area result from the ill-defined position of the central molecule inside the rectangular surface unit cell. On this primitive circle, two sets of four broad maxima are visible (one set is more intense than the other, indicated by arrows in Fig. 7(c)). The two intense  $(1, \bar{1})$  and  $(\bar{1}, 1)$  spots together with the four more intense broad maxima define a pseudo-hexagonal pattern. Note that only the diffraction spots of the rectangular lattice could be observed by LEED, and within a reduced energy range compared to the clean substrate (from 8 to about 100 eV of the primary electron beam), consistent with the quasi-ordered film structure. According to the adsorption energy calculations, the  ${}^4f B'_{hex}$  sites located at the center of a bipentagonal motif BP1 are the most favorable adsorption sites ( $E_{ad}=-3.31$  eV). If only this subset of adsorption was decorated by molecules, the corresponding FFT transform would consist of a sharp orthorhombic pattern. There would be one single molecule per rectangular surface unit cell and the NN distances between adjacent molecules would correspond to the unit mesh dimensions (*i.e.* 1.23 and 1.44 nm). These distances are much larger than the spacing  $R_0$  for which the intermolecular potential energy is minimized ( $\simeq 1$  nm). The observed additional diffuse intensity indicates that molecules can also be adsorbed at other sites. The next most stable adsorption site determined by DFT is a 5-fold site located in-between two bipentagonal motifs ( $E_{ad}=-3.02$  eV). The distance between one  ${}^4f B_{hex}$  type of site and adjacent stable 5-fold sites are either too short ( $\simeq 0.83$  nm) or too long ( $\simeq 1.2$  nm) compared to  $R_0$ . It would thus be unfavorable to have both sites occupied simultaneously because of intermolecular forces, due to either the repulsive or attractive part of the intermolecular potential. Therefore we believe that the film is only quasi-ordered because the distances between the most favorable adsorption sites are too large compared to the spacing  $R_0$  minimizing the intermolecular potential energy.

Finally, the electronic structure of the  $C_{60}$  film has been investigated by mean of ultraviolet photoemission spectroscopy (UPS). The valence band of the film deposited at 693 K is compared in Fig. 8 to those of the clean substrate and of a multilayer  $C_{60}$  film deposited at 300 K. The different peaks observed for the multilayer film correspond to the various molecular orbitals. The position of these molecular orbitals are roughly unchanged in the monolayer film, but they are significantly broader due to the hybridization with the substrate. The Co  $d$  states which dominates the substrate valence band should also contribute to the spectrum, in an energy range which overlaps with that of the highest occupied molecular orbital at about 2 eV.

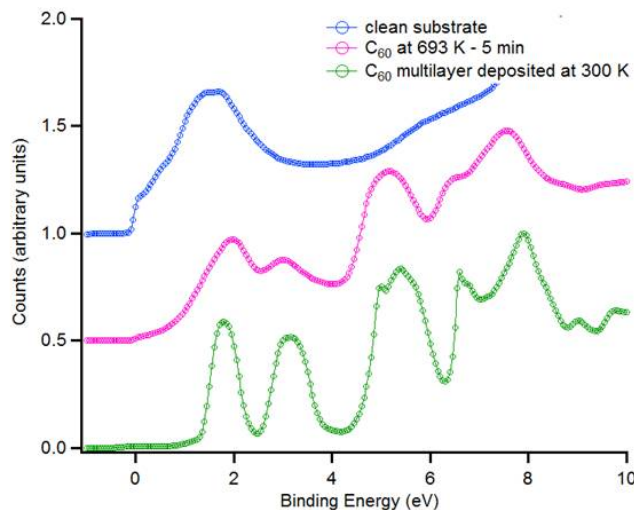


FIG. 8. UPS spectra of the clean substrate (top), of the  $C_{60}$  monolayer deposited at 693 K (middle) and of a multilayer  $C_{60}$  film dosed at 300 K.

### F. Carbide formation

As previously mentioned, a  $C_{60}$  monolayer deposited at room temperature is found to degrade after post-annealing at temperatures higher than 693 K as can be seen in the XPS core-level spectra shown in Fig. 9. The Al  $2p$  core-levels are slightly shifted by 0.2 eV towards higher binding energies upon dosing and annealing at 693 K. Annealing the film at higher temperatures leads to a broadening of the Al  $2p$  spectrum ascribed to the presence of an extra feature on the high binding energy side at about 73.65 eV.[29] In addition, a new component is also observed at 282 eV in the C  $1s$  spectrum upon annealing above 693 K. The intensity ratio of this additional component with respect to the main peak at 284 eV is growing with increasing annealing temperature as well as with annealing time. These changes in XPS core-level spectra are interpreted by the formation of aluminum carbide [29].

After annealing the film between 843 K and 1073 K, the LEED pattern shows substrate spots as well as a new ring having a radius equal to  $5c^*$  (Fig. 10). A second ring is also observed for higher electron beam energies. It corresponds to a hexagonal structure with lattice parameters  $a = 3.34 \text{ \AA}$  and  $\gamma = 120^\circ$ . A similar structure was reported for  $C_{60}$  films on related  $Al_9Co_2(001)$  surface [29] and is consistent with the formation of an aluminum carbide thin film ( $Al_4C_3$ ,  $R\bar{3}m$ ,  $a = 3.33 \text{ \AA}$  and  $b = 24.97 \text{ \AA}$ ,  $\gamma=20^\circ$ )[48]. The diffraction ring is essentially diffuse although some weak spots can be distinguished. The diffuse ring indicates that the hexagonal domains have a random azimuthal orientation with respect to the substrate. The weak spots suggest that some preferred orientation only starts to emerge under these experimental conditions.

## IV. DISCUSSION AND CONCLUSIONS

At submonolayer coverages and at room temperature, surface diffusion of isolated molecules is inhibited on the  $Al_{13}Co_4(100)$  surface. As a result, the complete monolayer grown at room temperature is disordered. This is consistent with previous studies of  $C_{60}$  films grown on related Al-based quasicrystals and complex metallic alloys. The surface terminations of these intermetallics consist in Al-rich plane, therefore it is worth comparing with the case of  $C_{60}$  films grown on Al surfaces. On all low-index surfaces of Al, the molecules are mobile at room temperature. Different phases have been reported. On Al(111), an ordered metastable  $(2\sqrt{3}\times 2\sqrt{3})R30^\circ$  phase is formed at room temperature deposition whereas upon annealing at 620 K a  $(6\times 6)$  phase is formed involving some reconstruction of the substrate [46]. Ordered phases are also formed on the Al(110) and Al(100) surfaces upon dosing at 620 K and 590 K respectively [46, 49]. For both (110) and (111) surfaces, covalent bonding interactions between the Al substrate and the molecule have been identified by spectroscopy methods. The calculated adsorption energies for  $C_{60}$  on  $Al_{13}Co_4(100)$  surface are rather large and spread in a range from about -1.5 eV to -3.3 eV. It indicates a corrugated potential energy surface compared to simple metal surfaces, thus preventing diffusion at room temperature. As a consequence, ordered molecular layers can only be formed at high deposition temperature. The  $C_{60}$  layers adopt the orthorhombic unit mesh of the substrate as evidenced by LEED and FFT of STM images ( $b \sim 1.23 \text{ nm}$



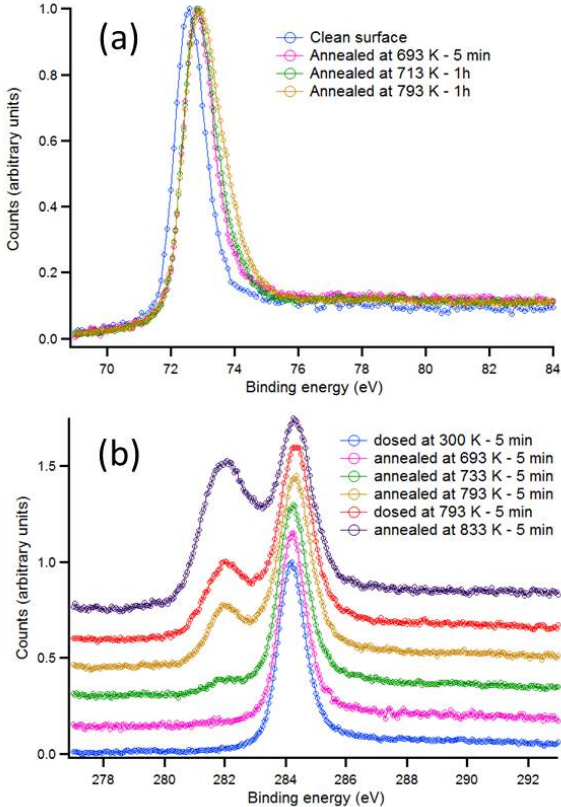


FIG. 9. (a) Al  $2p$  core-level spectra of the clean surface and after dosing and annealing a  $C_{60}$  monolayer. (b) C  $1s$  core-level spectra obtained after dosing a monolayer of  $C_{60}$  and annealing at various temperatures.

and  $c \sim 1.44$  nm). On a local scale, the film appears quasi-ordered only and additional diffuse diffraction spots are observed in FFT of STM images. The DFT calculations have identified two strong adsorption sites with relatively close adsorption energies. One corresponds to a  $C_{60}$  molecule positioned with one hexagonal face at the center of the BP1 motif. The second largest adsorption energies are found for a  $C_{60}$  adsorbed between the bipentagonal motifs with a pentagonal face parallel to the surface. These two sites cannot be occupied simultaneously as this would correspond to intermolecular distances too far apart from the the distance  $R_0$  minimizing intermolecular interactions, thus explaining the presence of some disorder in the molecular film. In order to estimate the packing density of the film, the average surface area per molecule was estimated by counting individual molecules. A value of  $0.95 \text{ nm}^2$  is deduced. This is slightly larger than the theoretical value based on an occupancy of 2 molecules per unit mesh ( $0.88 \text{ nm}^2$ ). This packing density is intermediate between that of quasiperiodic  $C_{60}$  films mentioned earlier ( $1 \text{ nm}^2$ ) [27] and that of  $C_{60}$  film on related  $Al_9Co_2(001)$  surface ( $0.91 \text{ nm}^2$ ) [29]. Attempts to grow molecular films at temperature higher than 693 K led to  $C_{60}$  decomposition and formation carbide thin films. This work indicates that molecular films with a variety of different structures can be obtained by using complex intermetallics as templates, where each molecule is strongly bounded to the substrate with a specific orientation, providing that the distances between the most preferred adsorption sites is compatible with the distance minimizing intermolecular interactions which is not precisely the case of the particular  $Al_{13}Co_4(100)$  surface.

## V. ACKNOWLEDGMENTS

This work was supported by the Lorraine Region, the joint ANR-DFG CAPRICE 2011-INTB 1001-01, the European C-MAC consortium and CNRS (INCAS project N° PICS05892). This work was granted access to the HPC resources



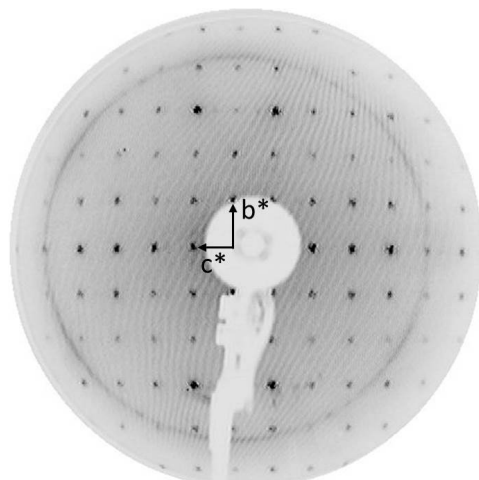


FIG. 10. LEED pattern at 53 eV beam energy of the carbide film formed by dosing  $C_{60}$  at 873 K and annealing up to 1073 K. The reciprocal unit mesh of the substrate is indicated. The diffuse intensity ring has a radius equal to  $5c^*$ .

of IDRIS under the allocation 2015096339.

- 
- [1] G. Cuniberti, K. Richter, and G. Fagas, *Lecture Notes in Physics*, Vol. 680 (Springer, Berlin, 2005).
- [2] M. S. Dresselhaus, G. Dresselhaus, and P. C. Eklund, *Science of Fullerenes and Carbon Nanotubes* (Academic Press, San Diego, 1996).
- [3] T. Sakurai, Q. Xue, T. Hashizume, and Y. Hasegawa, *J. Vac. Sci. Technol. B* **15**, 1628 (1997).
- [4] T. Hashizume, K. Motai, X. Wang, H. Shinohara, Y. Saito, Y. Maruyama, K. Ohno, Y. Kawazoe, Y. Nishina, H. Pickering, Y. Kuk, and T. Sakurai, *Phys. Rev. Lett* **71**, 2959 (1993).
- [5] L. Wang and H. Cheng, *Phys. Rev. B* **69**, 045404 (2004).
- [6] C. Cepek, A. Goldoni, and S. Modesti, *Phys. Rev. B* **53**, 7466 (1996).
- [7] M. Casarin, D. Forrer, T. Orzali, M. Petukhov, M. Sambì, E. Tondello, and A. Vittadini, *J. Phys. Chem. C* **111**, 9365 (2007).
- [8] S. W. M. A. J. Nakamura, T. Nakayama, *Phys. Rev. Lett.* **87**, 048301 (2001).
- [9] E. I. Altman and R. J. Colton, *Phys. Rev. B* **48**, 18244 (1993).
- [10] W. Pai and C. L. Hsu, *Phys. Rev. B* **68**, 121403 (2003).
- [11] H. I. Li, K. J. Franke, J. I. Pascual, L. W. Bruch, and R. D. Diehl, *Phys. Rev. B* **80**, 085415 (2009).
- [12] S. Guo, D. P. Fogarty, P. M. Nagel, and S. A. Kandel, *J. Phys. Chem. B* **108**, 14074 (2004).
- [13] J. E. Rowe, P. Rudolf, L. H. Tjeng, R. A. Malic, G. Meigs, C. T. Chen, J. Chen, and E. W. Plummer, *Int. J. Mod. Phys. B* **6**, 3909 (1992).
- [14] P. W. Murray, M. Ø. Pedersen, E. Lgsgaard, I. Stensgaard, and F. Besenbacher, *Int. J. Mod. Phys. B* **55**, 9360 (1997).
- [15] R. Felici, M. Pedio, F. Borgatti, S. Iannotta, M. Capozzi, G. Ciullo, and A. Stierle, *Nature Materials* **4**, 688 (2005).
- [16] T. Orzali, D. Forrer, M. Sambì, A. Vittadini, M. Casarin, and E. Tondello, *J. Phys. Chem. C* **112**, 378 (2008).
- [17] J. Weckesser, J. V. Barth, and K. Kern, *Phys. Rev. B* **64**, 161403 (2001).
- [18] X. Zhang, W. He, H. Li, L. Chen, W. W. Pai, J. Hoi, M. M. T. Loy, J. Yang, and X. Xiao, *Phys. Rev. B* **75**, 235444 (2007).
- [19] C.L.Henley, *J. Non-Cryst. Solids* **153-154**, 172 (1993).
- [20] R. Addou, E. Gaudry, T. Deniozou, M. Heggen, M. Feuerbacher, P. Gille, Y. Grin, R. Widmer, O. Gröning, V. Fournée, J. Dubois, and J. Ledieu, *Phys. Rev. B* **80**, 014203 (2009).
- [21] H. Shin, K. Pussi, É. Gaudry, J. Ledieu, V. Fournée, S. Alarcón-Villaseca, J.-M. Dubois, Y. Grin, P. Gille, W. Moritz, and R. Diehl, *Physical Review B* **84**, 085411 (2011).
- [22] V. Fournée, E. Gaudry, M.-C. de Weerd, R. D. Diehl, and J. Ledieu, *Mater. Res. Soc. Symp. Proc.* **1517**, 1570 (2012).
- [23] J. Ledieu, C. Muryn, G. Thornton, R. Diehl, T. Lograsso, D. Delaney, and R. McGrath, *Surf. Sci. Lett.* **472**, 89 (2001).
- [24] E. Cox, J. Ledieu, V. Dhanak, S. Barrett, C. Jenks, I. Fisher, and R. McGrath, *Surf. Sci.* **566-568**, 1200 (2004).
- [25] J. Smerdon, L. Leung, J. Parle, C. Jenks, R. McGrath, V. Fournée, and J. Ledieu, *Surf. Sci.* **602**, 2496 (2008).
- [26] J. A. Smerdon, *Journal of Physics: Condensed Matter* **22**, 433002 (2010).
- [27] V. Fournée, E. Gaudry, J. Ledieu, M. C. de Weerd, D. Wu, and T. A. Lograsso, *ACS Nano* **8**, 36463653 (2014).

- [28] J. A. Smerdon, K. M. Young, M. Lowe, S. S. Hars, T. P. Yadav, D. Hesp, V. R. Dhanak, A. P. Tsai, H. R. Sharma, and R. McGrath, *Nano Letters* **14**, 1184 (2014).
- [29] J. Ledieu, E. Gaudry, M.-C. de Weerd, P. Gille, R. D. Diehl, and V. Fournée, *Phys. Rev. B* **91**, 155418 (2015).
- [30] T. Goedecke and M. Ellner, *Z. Metallkd.* **87**, 854 (1996).
- [31] P. Gille and B. Bauer, *Cryst. Res. Technol.* **43**, 1161 (2008).
- [32] I. Horcas, R. Fernandez, J. M. Gomez-Rodriguez, J. Colchero, J. Gomez-Herrero, and A. M. Baro, *Review of Scientific Instruments* **78**, 013705 (2007).
- [33] G. Kresse and J. Hafner, *Phys. Rev. B* **47**, 558 (1993).
- [34] G. Kresse and J. Hafner, *Phys. Rev. B* **49**, 14251 (1994).
- [35] G. Kresse and J. Furthmüller, *Phys. Rev. B* **54**, 11169 (1996).
- [36] G. Kresse and J. Furthmüller, *Computational Materials Science* **6**, 15 (1996).
- [37] P. Blöchl, *Phys. Rev. B* **50**, 17953 (1994).
- [38] G. Kresse and D. Joubert, *Phys. Rev. B* **59**, 1758 (1999).
- [39] J. P. Perdew, K. Burke, and M. Ernzerhof, *Phys. Rev. Lett.* **77**, 3865 (1996).
- [40] J. P. Perdew, K. Burke, and M. Ernzerhof, *Phys. Rev. Lett.* **78**, 1396 (1997).
- [41] J. Grimme, *J. Comput. Chem.* **27**, 1787 (2006).
- [42] J. Grin, U. Burkhardt, M. Ellner, and K. Peters, *J. Alloys Comp.* **206**, 243 (1994).
- [43] J. A. Smerdon, J. K. Parle, L. H. Wearing, L. Leung, T. A. Lograsso, A. R. Ross, and R. McGrath, *J. Phys.: Conf. Ser.* **226**, 012006 (2010).
- [44] H. Shin, A. Schwarze, R. D. Diehl, K. Pussi, A. Colombier, E. Gaudry, J. Ledieu, G. M. McQuirk, L. N. Serkovic Loli, V. Fournée, L. L. Wang, G. Schull, and R. Berndt, *Phys. Rev. B* **89**, 245428 (2014).
- [45] J. A. Larsson, S. D. Elliott, J. C. Greer, J. Repp, G. Meyer, and R. Allenspach, *Phys. Rev. B* **77**, 115434 (2008).
- [46] A. Maxwell, P. Brühwiler, D. Arvanitis, J. Hasselström, M.-J. Johansson, and N. Mårtensson, *Phys. Rev. B* **57**, 7312 (1998).
- [47] M. H. K. Ji Young Lee, *Surf. Sci.* **602**, 1408 (2008).
- [48] T. M. Gesing and W. Jeitschko, *Z. Naturforsch. B* **50b**, 196 (1995).
- [49] R. Fasel, P. Aebi, R. G. Agostino, D. D. Naumovic, J. Osterwalder, A. Santaniello, and L. Schlapbach, *Phys. Rev. Lett.* **76**, 4733 (1996).